Thin-layer approximation for the multi-physics and multiscale simulation of cell membrane electrodeformation

Elias Sabri, Christian Brosseau

Version of Record: https://www.sciencedirect.com/science/article/pii/S1567539422000068
Manuscript_3bd78a252580fa5e5cce4d259a4e3adf

Thin-layer approximation for the multi-physics and multiscale simulation of cell membrane electrodeformation

E. Sabri and C. Brosseau*

Univ Brest, CNRS, Lab-STICC, CS 93837, 6 avenue Le Gorgeu, 29238 Brest Cedex 3, France

* Email: brosseau@univ-brest.fr

ABSTRACT

Multi-physics simulation techniques provide a platform that is used to gain insights into complex biological problems with multiple length scales such as cell electrodeformation (ED) and electropermeabilization (EP). However, owing to the large degrees of freedom required to compute the electromechanical properties at very different length scales (membrane thickness, cell size, and customized tissue scaffold) finite element (FE) simulations can be computationally very expensive. Here, we report on a general method of analysis by which we can systematically simulate multiscale ED under direct-current electric fields. In the context of electromechanical continuum behavior, the key novelty of our work is the introduction of a specific Dirichlet boundary condition, i.e. thin-layer approximation (TLA), to represent the capacitive elastic cell membrane. To test the robustness of this newly proposed procedure, Maxwell stress tensor (MST) and cell displacement arising from ED forces obtained with the TLA are compared with a model using a physical thickness of the cell membrane. Furthermore, we present our results in terms of benchmark points for vesicle deformation induced by an electric field excitation and we confirm our approximate results are relevant to predict the aspect ratio characterizing the ellipsoidal deformation of an initially spherical vesicle.

Keywords: Finite element analysis, cell membrane, electrodeformation, multi-physics multiscale simulations, boundary conditions

I. INTRODUCTION AND MOTIVATION

The inherent complexity of biomaterials is well recognized; they are multi-scale, multi-science systems, and bridging a wide range of temporal and spatial scales [1-6]. In the context of computational analysis of cell membrane, it is known that its heterogeneity and anisotropy can substantially impact physical properties such as the permeabilization under various exogeneous field excitations [4-17]. This challenge is further elevated for a core-shell modelling of cell that undergo large deformations under electromechanical excitation [7,13-18]. Because of all of these features, finite element (FE) simulations are a method of choice to explore how the cell effective properties emerge from local molecular features and how the interplay among its numerous components gives rise to function over spatial and time scales much larger than the molecular ones. However, a comprehensive understanding of the interplay between the electromechanical coupling and membrane deformation-permeabilization remains incomplete [6-10].

The core (cytoplasm)-shell(membrane) structure, i.e. a dielectric nanometric membrane surrounded by conducting cytoplasm and extracellular medium (ECM), has been quite successful, notably for evaluating the transmembrane potential (TMP). An overview of models and numerical schemes for the core-shell description is provided in [3]. While this model is an important object of study that features various electromechanical properties of cell membrane it is likely too simplified to describe real biological cells. Simulations, until now, have largely focused on a rather narrow picture of the complexity of the membrane (dielectric, elastic continuum object). However, as FE simulations are becoming increasingly sophisticated, the most widely used methods used to analyze ED and EP issues exposes serious drawbacks in dealing with electromechanical properties at very different length scales (membrane thickness, cell size, and customized tissue scaffold) and need to be improved. This is especially true for multiscale problems that require frequent remeshing to track large structural deformations, i.e. upon application of an electric field energy does redistribute to maintain consistency boundary conditions through a perturbation of line fields. Furthermore, this feature renders the computation very costly in terms of computation time and memory requirements. Correspondingly, many new ways of testing for the properties of membrane ED and EP have yet to be explored.

In addition, there is the added complexity involved in dealing with the study of multiple interacting physical properties, i.e. electromechanical coupling [3,11]. Over the years, the literature suggests several ways which can be implemented numerically, and a general approach is illustrated in Fig. 1(a).

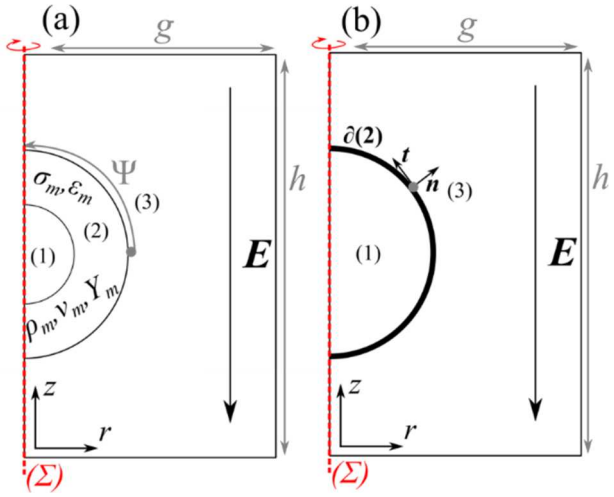

Fig. 1: (a) Exact geometry of our composite model with the physical membrane (full model (FM)). The stress (force per unit area) is directed from the dielectric with a higher permittivity (cytoplasm and ECM) towards the dielectric with a lower permittivity (membrane). Components (1), (2), and (3) represent respectively the cytoplasm, membrane, and ECM. In the cylindrical coordinate system, any point of the *xOy* Cartesian plane can be described via a single *r* coordinate as axisymmetric conditions are assumed for the rectangular computational domain, where *g* and *h* are the dimensions along the *z* and *r* directions respectively. The electric field is oriented along the *z*-direction, ψ denotes an angle relative to the electric field direction. The application of an electric field is performed using Dirichlet boundary conditions on top and bottom horizontal surfaces such as $V(z=0)=0$ and $V(z=h)=E.h$, where *E* denotes the applied field modulus; (b) As in (a) for the TLA-based approach: the idea is to replace the exact physical conditions by approximate numerical conditions that connect the solution on the two sides of the homogeneous thin-layer (physical membrane) boundary, therefore avoiding the need to mesh the layer and solve the exact ED problem, ***t*** and ***n*** denote respectively the unit vectors characterizing the local tangential and normal directions. The computational box is assumed to be relatively large ($h=10R$, $g=5R$) in each configuration, where *R* denotes the cell (vesicle) radius (in the undeformed state).

In the case of discretizations based on FE, the dominant error is due to the mesh adaptation scheme used in the simulations. In the context of continuum scale theory, one elegant approach consists to solve large heterogeneous structures without scale separation assumption by introducing relevant Dirichlet boundary conditions which can be satisfied on the capacitive elastic membrane. There have been several attempts to address this question, particularly in the context of electric characterization of cell membrane. To perform TMP, V_m, calculations on realistic cell shapes, Pucihar and coworkers [19] put forward a model to replace the membrane by a boundary condition on the cytoplasm. Since it avoids meshing the membrane this approximation permits a significant decrease of the computational time, discretization cost and used memory for the calculations. Another more recent variational approach for calculating the spatial distribution of electric field without meshing the membrane is seen in [20]. In [21], the ED dynamics of lipid vesicles under direct current electric field excitation is investigated where the vesicle membrane is represented as a massless immersed boundary. In [7,22-24], the immersed boundary method is used to simulate the ED and electrohydrodynamics of a vesicle in Navier-Stokes leaky dielectric fluids under various electric field excitations. The vesicle membrane is modeled as an inextensible elastic interface which is characterized by electric capacitance and conductance. Within the leaky dielectric framework and the piecewise constant electric properties in each

fluid, the electric stress can be treated as an interfacial force so that both the membrane electric and mechanical forces can be formulated within this immersed boundary method. Within another context, it was argued in [25] that TLA provides an alternative route to modelling dielectric spectra of biological cells.

In any event, it would appear that, while the construction of these boundary methods is a remarkable result, the fact that only the electric constraints are dealt with somewhat limits their potential for ED investigations [9-10]. For this reason, we introduce and validate a complementary and generic approach for simulating electromechanical phenomena that enables the simulation of models spanning several spatial and temporal scales. In this setting, explicit boundary conditions are enforced directly on the capacitive elastic cell membrane which is subjected to a direct-current electric field. We must remark that this approximation is not limited to direct-current problems but the conclusions reached in this paper apply quite generally to time-oscillating electric field with frequency up to 100 MHz. One of the primary determinants in describing the ED behavior is the Maxwell stress tensor (MST) driving cytoplasmic remodeling under electric field excitation. However, how does such boundary conditions correlate with the quadratic variation of the MST as a function of V_m and cell displacement arising from ED forces have not seen much light. With this caveat in mind, the key novelty of our work is the introduction of an explicit thin-layer approximation (TLA) to simultaneously solving the electrical potential and calculating the MST and cell displacement. Here, an important advantage is that the geometries can be arbitrarily thin while permitting arbitrarily large structural deformations. An additional aim of the present work is to compare suitable characteristics of TLA-based models to those using physical thickness, i.e. for which one needs to geometrically resolve the thin layer, in terms of accuracy, efficiency, and computational time. Normally, we think of two analyses as being equivalent if they make identical predictions, all things otherwise being equal. We will argue that, remarkably, the computational time (resp. stability) is significantly lower (resp. higher) for the TLA-based models investigated.

The rest of the paper proceeds as follows. Section II is the main part of the study which sets forth the governing equations and outlines the numerical architecture of the FM model along with the basic computational TLA-based framework in terms of a continuum scale problem. Section III then details benchmark simulation test cases and compares results using a FM model to those using TLA to test the robustness of our results. Results obtained with the current method are compared in terms of accuracy, efficiency, and computational time. In Section IV, concluding remarks are stated and an outlook is provided. Finally, appendix A contains a technical note where we point out essential details, such as the type of electric pulse excitation and the geometry of each model, along with a few comparison cases of low-resolution quality outputs inherent to FM model versus high-resolution quality outputs of the TLA model, when modeling ED for a multi-cell system.

II. THIN-LAYER APPROXIMATION OF CAPACITIVE ELASTIC CELL MEMBRANE

Here, we outline the physics for readers not familiar with the field and describe our geometric configuration, introducing the notation and terminology of the model. We first set the theoretical basis of our analysis and then present the numerical procedure which is implemented for performing electrically-induced cell deformation calculations based on MST computation.

A. The mathematical setup

We begin by making some simple observations about the polarizable and deformable continuum model. In this paper, we consider the morphology of an initially (undeformed) spherically-shaped cell. In particular, we investigate its ellipticity and whether it might be prolate or oblate under electric field excitation. In this context, we assume that cells remain spheroidal under a slowly varying direct current (or quasistatic time-oscillating) electric field. Furthermore, we assume three independent phases (cytoplasm, membrane, and ECM) with permittivity, electrical conductivity, elastic modulus and Poisson ratio described by piecewise constants on either side of the interface. We should point out that in developing our approach we do not address the details of the material behavior, including effects related to the molecular structure. The parameter used for the numerical examples are those employed earlier [26] and are listed in Table I (appendix A). A convenient way to describe the force density on the membrane due to the electrostatic interaction is to use MST calculations [6-7,19-24,26-28]. The quadratic dependence of the ED force here makes this step essential in our simulations since in general it is useful to impose V_m<1 V to avoid EP [12-13,26].

Our analysis focuses on two different cell configurations comprising either a single cell (2D axisymmetric geometry shown in Fig. 1) or two cells (3D geometry displayed in Fig. S2). The displacement is modelled by applying an electric field along the z direction. The calculation of the electrical part of the simulation is being realized by making use of the following set of governing equations

$$\sum_i \partial_i J_i - \partial\rho/\partial t = 0, \tag{1}$$

$$J_i=\sigma E_i+\partial D_i/\partial t, \tag{2}$$

$$E_i=-\partial_i V, \tag{3}$$

$$T_{ij}=\varepsilon\varepsilon_0 \left(E_i E_j - \frac{1}{2}\delta_{ij}E_i^2\right), \tag{4}$$

where indices i,j = {r,z} for 2D axisymmetric geometry (see Fig. 1) and i,j = {x,y,z} for 3D geometry (see Fig. S2). All quantities above are time dependent and defined as follows: T is Maxwell stress tensor, E is the electric field, D is the electric displacement, δ is the Kronecker's delta, σ means the electrical conductivity, ε is the permittivity, V is the electric potential, J is the electric current density, ρ is the volume charge density, and t denotes the time. At membrane interfaces, one can express any of these quantities as a function of the normal and tangential directions by setting $i,j = \{n,t\}$ for 2D geometry and $i,j = \{n,t_1,t_2\}$ in 3D geometry. All materials being assumed to be isotropic, conductivities and permittivities are represented by scalars. The boundary conditions at the interface between any two adjacent regions (noted A and B referring to any pair of domains (1), (2) or (3) shown in Fig. 1(a)) can be expressed in vector notation as

$$\boldsymbol{n}.(\boldsymbol{J}_A-\boldsymbol{J}_B)=\partial\rho_s/\partial t\ , \tag{5}$$

$$\boldsymbol{n}.(\boldsymbol{D}_A-\boldsymbol{D}_B)=\rho_s\ , \tag{6}$$

$$\boldsymbol{t}.(\boldsymbol{E}_A-\boldsymbol{E}_B)=0. \tag{7}$$

Here ρ_s denotes the electric charge surface density and $\boldsymbol{n}$ and $\boldsymbol{t}$ respectively account for the normal and tangential vectors to the boundary which is considered. On the other hand, the set of equations previously described is to be supplemented by the mechanical part of the simulations, which is based on the outputs of the previous stage

$$\sum_i \partial_i S_{ij} = -\rho(\partial^2 u_i/\partial t^2)\,, \tag{8}$$

$$S_{ij} = \sum_{\boldsymbol{k}} \sum_{\boldsymbol{l}} C_{ijkl}.\kappa_{kl}, \tag{9}$$

$$\kappa_{ij} = \frac{1}{2}[\partial_i u_j + \partial_j u_i], \tag{10}$$

where S is the Cauchy stress tensor, C is the compliance tensor, κ is the strain tensor, ρ is the density, and u denotes the displacement vector. An important point is to note that the acceleration term $\rho(\partial^2\boldsymbol{u}/\partial\boldsymbol{t}^2)$ in the momentum equation can be neglected since the viscous relaxation time is smaller than the changes in the applied electric field [14]. Thus, based on the problem is treated quasi-statically and Eq.(8) can be approximated as

$$\sum_i \partial_i S_{ij} = 0\,. \tag{11}$$

Furthermore, according to the theory of linear elasticity and since the membrane and cytoplasm are assumed to be isotropic materials, the compliance tensor C_{ijkl} can be described by three different terms ($C_{iiii}, C_{ijij}, C_{iijj}$, whereas other terms are zero) which depend on the Young modulus (Y) and Poisson ratio (ν). These terms can be written as

$$C_{iiii} = \frac{Y(1-\nu)}{(1+\nu)(1-2\nu)} \tag{12}$$

$$C_{iijj} = \frac{Y\nu}{(1+\nu)(1-2\nu)} \tag{13}$$

$$C_{ijij} = \frac{Y}{2(1+\nu)} \tag{14}$$

Although there has been a good deal of attention directed towards calculating TMP, relatively few studies have analyzed the electromechanical coupling. This omission is partly due to the fact that only simple geometrical cell shapes were considered and that the knowledge of full morphological information is elusive without precise 3D spatial and kinematic data for cell assemblies [34-36]. In the following, we develop an analytical approach for calculating the components of the electric field from which we subsequently evaluate the MST onto the membrane surface. We will provide a comparative analysis between FM and TLA models to validate the accuracy of the latter approach. For illustrative purpose, we compare in Fig. 1 the geometrical configuration with three distinct domains for the FM model with its counterpart for the TLA model characterized by two domains and an effective boundary condition that replaces component (2).

Several remarks are in order. Firstly, in the case of a non-planar membrane, the continuity equation, Eq.(1), inside the membrane implies a slight difference in the electric field values at its interfaces between domains (1)-(2) and (2)-(3) displayed in Fig. 1(a). The electric field vector on the former is noted as $\boldsymbol{E}_{(2)-}$ while the electric field vector on the latter is written as $\boldsymbol{E}_{(2)+}$. Interestingly, FM results show that both ED and membrane compression mostly arise from the imbalance of the MST inside the membrane at these two interfaces. Consequently, an important and yet complex feature for a rigorously equivalent TLA model lies in the accurate computation of the MST on each internal interfaces of the membrane, which necessitates an accurate computation of the electric field that relates to MST, i.e. Eq.(4). For this purpose, we introduce two quantities in the TLA model, namely $\boldsymbol{E}_{\partial(2)+}$ and $\boldsymbol{E}_{\partial(2)-}$ which are equivalent respectively to $\boldsymbol{E}_{(2)-}$ and $\boldsymbol{E}_{(2)+}$ in the FM model. We also define appropriate boundary conditions for the normal and tangential components of the electric field vector on the membrane

$$\boldsymbol{t}.\boldsymbol{E}_{\partial(2)-} = \boldsymbol{t}.\boldsymbol{E}_{(1)}, \tag{15}$$

$$\boldsymbol{t}.\boldsymbol{E}_{\partial(2)+} = \boldsymbol{t}.\boldsymbol{E}_{(3)}, \tag{16}$$

$$\boldsymbol{n}.\boldsymbol{E}_{\partial(2)-} = \Gamma_1\, \boldsymbol{n}.\boldsymbol{E}_{\partial(2)+} = \Gamma_2\, V_m/d_m. \tag{17}$$

In Eq. (14), Γ_1 and Γ_2 account for the electric field gradient across the membrane, where the value of the normal component of the electric field at any point within a spherical membrane can be computed from the expression $V_m/d_m\left(\frac{(R-x)^2}{(R-d_m/2)^2}\right)$, where x represents the distance to the outer surface of the membrane. The two parameters Γ_1 and Γ_2 in Eq.(14) can be written as $\Gamma_1 = \left(\frac{R^2}{(R-d_m)^2}\right)$ and $\Gamma_2 = \left(\frac{(R-d_m/2)^2}{(R-d_m)^2}\right)$. Additionally, from Eq. (14) we observe that the average value of the electric field imbalance at any two points of the normal direction on the membrane is well approximated by V_m/d_m as long as the geometry of the problem satisfies $R>>d_m$. The time dependent governing equations are then solved for the TLA model with two boundary conditions for the electrical part

$$\boldsymbol{n}\,.\boldsymbol{J}_{(1)} = \frac{1}{d_m}\left(\sigma_m + \epsilon_m\epsilon_0\frac{\partial}{\partial t}\right)\left(V_{(1)} - V_{(3)}\right), \tag{18}$$

$$\boldsymbol{n}\,.\boldsymbol{J}_{(3)} = \frac{1}{d_m}\left(\sigma_m + \epsilon_m\epsilon_0\frac{\partial}{\partial t}\right)\left(V_{(3)} - V_{(1)}\right). \tag{19}$$

The mechanical part of the TLA model is dealt with the standard shell deformation theory

$$S_{ij}{}^{m} = \sum_{\boldsymbol{k}}\sum_{\boldsymbol{l}} C_{ijkl}.\kappa_{kl}{}^{m}, \tag{20}$$

$$S_{ij}{}^{b} = \frac{\boldsymbol{d_m}}{\boldsymbol{2}}\sum_{\boldsymbol{k}}\sum_{\boldsymbol{l}} C_{ijkl}.\kappa_{kl}{}^{b}\,, \tag{21}$$

$$S_{ij}{}^{s} = \frac{\boldsymbol{5}}{\boldsymbol{6}}\sum_{\boldsymbol{k}}\sum_{\boldsymbol{l}} C_{ijkl}.\kappa_{kl}{}^{s}\,, \tag{22}$$

$$S_{ij}{}^{in-plane} = S_{ij}{}^{m} + \zeta_n\, S_{ij}{}^{b}, \tag{23}$$

$$6\frac{\zeta_n}{\boldsymbol{d_m}}(\boldsymbol{M}\times\boldsymbol{n}) + \sum_i \partial_i\, S_{ij}{}^{in-plane} = 0\,, \tag{24}$$

where the exponents m, b, and s respectively denote the membrane, bending and shear associated to either stress or strain, ζ_n represents the space coordinate within the membrane in the normal direction, $\boldsymbol{M}$ is the bending moment , $\boldsymbol{n}$ is the normal vector**,** and $\times$ represents the vector product operator. In the set of Eqs. (20)-(24), we exclusively consider in-plane strains for which the normal component of the strain $\kappa_{nn}$is assumed to be not relevant, i.e. electrostriction is neglected.

B. Numerical procedure

The purpose of this section is to give a detailed overview of the numerical methods used to run the FM and TLA models. We start by briefly presenting the FE method used to solve the sets of equations presented in the previous subsection before introducing the mathematical formalism used to reduce the set of equations down to a 1-variable problem which is numerically solved. Then, we comment on the mesh construction procedure. Finally, we offer a brief analytical description of the FE method for solving the present multi-physics problem. The details of the convergence analysis for each model are relegated to Appendix A.

Simulations were performed using the multi-physics COMSOL software [37] and were run in a cluster computer (262 GB RAM, Intel® Xeon® 2.2 GHz (48 CPUs) processor). As previously mentioned, the cell components displayed in Fig.1(a) are represented by continuous media which are meshed in order to solve the continuum physics equations. As first step, a mesh of the system created, i.e. each domain is discretized into building-blocks subdomains, i.e. FEs. Then, polynomial functions (called shape functions) are introduced to approximate the exact solution in each FE. The order of these shape functions is called the discretization order. Additionally, in COMSOL, in order to optimize the accuracy of the solution for complex geometries, geometric shape functions are used to mesh the system, i.e. for any curved surface the geometry is approximated by a polynomial function of the same discretization order as the one considered in the physical problem. This is meant to optimize the agreement between the exact and computed solution at a sub nodal scale. Since discretization for the electrical and mechanical parts of the algorithm is performed independently, the geometrical shape functions are set to the lowest defined discretization order in multi-physics problems. Two different types of mesh can be constructed depending on the geometry of the problem to be solved, either a structured or an unstructured mesh. The former requires a relatively simple geometry and is less computationally expensive as regularity allows storage arrangements of neighborhood relationships between nodes. The former implies explicit storage of neighborhood relationships but at the same time allows meshing virtually any type of geometry. The geometry of the simulated system can then be meshed using elements of different morphologies: linear elements for 1D geometries, triangular or quadrilateral elements for 2D geometries, and either tetrahedral, pyramidal, prismatic or hexahedral elements for 3D geometries, each of which being more or less adapted depending on the topology of the system. Here, since we consider a multi-scale combination of circular and rectangular topologies (respectively, the membrane and the simulation box) we chose to use unstructured meshes of triangular elements to discretize the 2D axisymmetric geometries of FM and TLA models represented in Fig. 1, and tetrahedral elements for the 3D geometries of FM and TLA models sketched in Fig. A2. The element shape order was set to be quadratic to optimize the balance between accuracy and computational time since linear shape order elements would have implied over refining the mesh to achieve the same accuracy over the curved geometry of the membrane and higher shape order elements would have resulted in larger computational times. The equations are then solved using a multifrontal massively parallel sparse direct solver and based on the damped Newton's nonlinear method with a constant damping factor set to 1. Time dependence was handled using a backward differentiation formula (BDF) time stepping method, where free time steps were taken by the solver and maximum and minimum allowed degrees of the interpolating polynomial of the BDF method were respectively set to 5 and 1. The order of computation of the various quantities is illustrated in Fig. 2 by arrows. The calculation consists in solving the partial differential equation which is derived by combining Eqs. (1)-(3)

$$\sum_i \partial_i\left(\sigma\partial_i + \epsilon\,\partial/\partial t\right)V - \epsilon\,\partial\left(\sum_i \partial_i{}^2 V\right)\Big/\partial t = 0\,, \tag{25}$$

which is solved for V. Then, J, E, D and T can be obtained from Eqs. (1)-(3). As mentioned before, solving Eq. (25) is approximated by shape functions, each one being specific to its associated element. The shape functions of order k (noted $P_k()$) are determined in the electrical part of the calculation by setting the polynomial coefficients to values that cancel the integral of electric power volume density in each element

$$\iiint_{V_{elem}} \sum_i \left(J_i\, P_2(\partial_i V_i)\right) dV = 0. \tag{26}$$

The mechanical part of the calculation is done by solving Eqs.(9)-(10) which satisfy

$$\iiint_{V_{elem}} S_{ij}\left(\sum_i P_2(u_i)\,{}^{\partial}/_{\partial u_i}\left(\kappa_{ij}\right) + \sum_i P_2(\partial_i u_i)\,{}^{\partial}/_{\partial(\partial_i u_i)}\left(\kappa_{ij}\right)\right)\ dV = 0. \qquad (27)$$

It is also worth noting that the electromechanical coupling is performed in the TLA model by making use of the arbitrary Lagrangian-Eulerian formulation for solving the time variation of the electric potential as the cell geometry is deforming.

Practically, the algorithm which is implemented is displayed in Fig. 2.

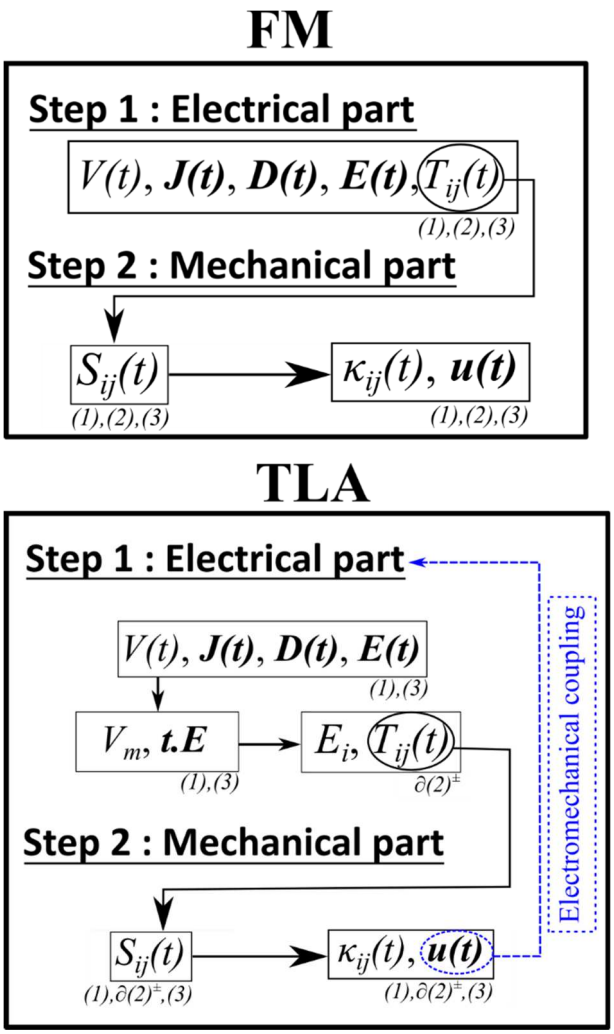

Fig. 2: Algorithm for computing cell deformation in TLA and FM models and calculating the ED coupling in the TLA model. Both models follow the same steps. Solving of the electrical part is followed by considering the mechanical part. The arrows illustrate the input versus output causal relationships of the algorithm. The blue arrow which represents the electromechanical mechanical coupling before shape change and electric potential calculation is implemented only in the TLA model.

Since we want to provide a comparison between FM and TLA models in terms of precision and computational time, a convergence study is performed. Since cell ED comes from MST imbalance across the membrane, our convergence criterion is defined with respect to the imbalance of the T_{nn} component of MST. Results are shown in Fig. A3 and discussed in Appendix A. Another motivation for defining this criterion as the salient indicator of mesh resolution optimization is the quadratic dependence of MST components on the electric field whose gradient is extremely sharp at the membrane interface, making this criterion the most

ill-conditioned quantity of interest in the presented model, and thus the most relevant for investigating convergence.

III. EXAMPLES AND DISCUSSION

We are now in a position to try to put everything together and present several numerical examples in order to demonstrate the accuracy and efficiency of the TLA for representing cell membrane. The electric stimulus is shown in Fig. A1 of Appendix A. Table II of appendix A lists the material properties of actual cells which have been deduced from consolidated literature data and includes the electric pulse characteristic times. As previously described, we perform our analysis in two ways. The cell membrane was defined with a boundary condition in the TLA model or with a physical thickness in the FM model. In the latter case, the mesh generator is able to mesh the membrane domain but the number of mesh elements must be much larger than in the TLA model to achieve the same precision (Table I). To check the agreement between both models we focus on the norm of the electric field, the value of the T_{nn} component of the MST on the membrane of the reference cell, and the transmembrane imbalance of these quantities. Considering that it is the transmembrane imbalance in these two quantities that determine the magnitude of the net electromechanical stress responsible for membrane deformation, we stress the importance of replicating not only the local values of electric field and MST, but also the values of their local transmembrane imbalance. In Fig. 2, we present a quantitative comparison of these quantities calculated by making use of either TLA- and FM-based approaches as function of angle ψ for a 1-cell configuration (reference cell in Fig. A2 displayed in appendix A).

It is worth noting that the two models give very similar numerical data in terms of electric field and T_{nn} component of the MST distribution, with TLA allowing much lower values of mesh elements and computational time (Table I). The average error is defined as $\frac{\int_{C_{ref.cell}} \chi_{FM} - \chi_{TLA} dl}{\int_{C_{ref.cell}} \chi_{FM} dl}$, where $\int_{C_{ref.cell}} dl$ represents the integral over the cell contour for a 2D geometry or over the reference cell contour taken at $\varphi = 0$ for the 3D geometry. For the FM model, the average error is found to be 0.58 % for the electric field imbalance and 0.2 % for the T_{nn} component imbalance, while the counterparts for the TLA model are respectively 0.16% for the electric field and 0.2% for the T_{nn} imbalances. The electric field and MST values are obtained with significant gains in computational time, i.e. by a factor of 18 for the time-dependent study related to Fig. 3 (for which only the electrical part is computed), a factor of 23 for the data related to Figs. 5 and 6 (for which the electrical and mechanical parts are simultaneously computed), and a factor of 15 for the results shown in Fig. 7.

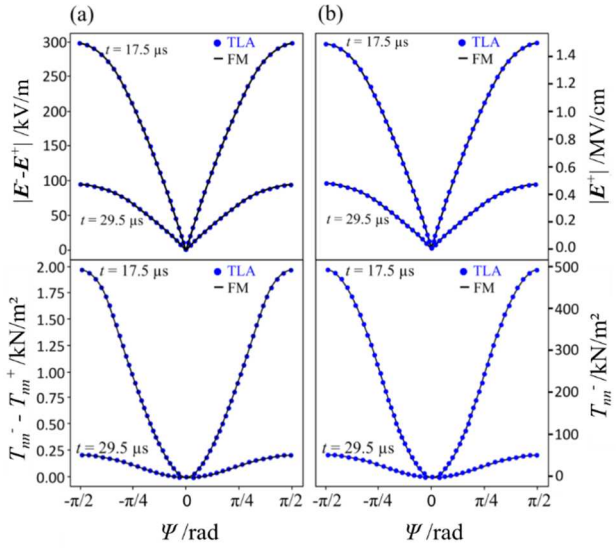

Fig. 3: (a) (top panel) Comparison between the angular variation in the transmembrane imbalance of the norm of the electric field between FM and TLA models for the 1-cell configuration at two times; (bottom panel) the same as in (top panel) for the transmembrane imbalance of T_{nn}; (b) (top panel) The same as in (a) in the top panel for the electric field on the boundary separating domain (2) from domain (3) of Fig. 1(a); (bottom panel) The same as in (b) in the top panel for T_{nn} on boundary separating domain (2) from domain (3) of Fig. 1(a), where exponents "+" and "-" respectively correspond to quantities related to boundaries separating domain (2) from domain (3) and domain (1) from domain (2) of Fig. 1(a).

To get further insight into the accuracy of the TLA model when one is dealing with cell assemblies under electric field excitation, we consider a 2-cell configuration (with reference to Fig. A2 of appendix A) since proximity interactions can in principle give important contributions. We illustrate these results in Fig. 4. The general features of the results deserve comments. These plots compare, as in Fig. 3, calculations of the intensity of the local electric field using TLA and FM approaches as function of angles ψ and φ for different relative cell orientations (characterized by angle θ in Fig. A2) to the electric field direction and inter-cellular distances (r/R with reference to Fig. A2). One observes that the trend of the curve obtained from the FM-based approach is well reproduced with TLA-based calculations for each configuration. Again, the main difference between the two models is the modest computational time (Table I) required to obtain the results for TLA-based simulations.

Table I: A comparison of several computational metrics at grid independence for the data shown in Figs. 3 and 4. The element quality is a measure of the good conditioning of the discretized problem and has a value comprised between 0 (inverted element) and 1 (perfect element). It is defined from the isotropy of the element divided by the condition number (Frobenius norm) of the matrix transforming the element to a perfect element. The element area (respectively volume) ratio corresponds to the smallest element area (respectively volume) divided by the largest.

	FM		TLA	
	1-cell (2D)	2-cell (3D)	1-cell (2D)	2-cell (3D)
Total number of mesh elements	1.49×10^5	9×10^6	1.09×10^3	9.79×10^4
Number of membrane mesh element	1.37×10^4	7.41×10^5	31	1.09×10^3
Degrees of freedom solved	3×10^5	1.2×10^7	2.3×10^3	1.8×10^5
Computational time	3 min 1s	26 min 48s	10 s	40 s
Mean element quality	0.97	0.77	0.97	0.82
Mean element quality (everywhere but membrane)	0.97	0.83	0.97	0.83
Minimum element quality (everywhere but membrane)	0.73	0.3	0.84	0.88
Mean element quality (membrane)	0.9	0.13	1	0.98
Minimum element quality (membrane)	0.87	0.0026	1	0.85
Element area ratio	5×10^{-9}	-	1.1×10^{-3}	-
Element volume ratio	-	1.2×10^{-10}	-	1.1×10^{-3}

Thus, the key point to take away is that TLA is a good candidate for exploring how the redistribution of field and force is reflected in symmetry breaking characterizing multiple cell configurations.

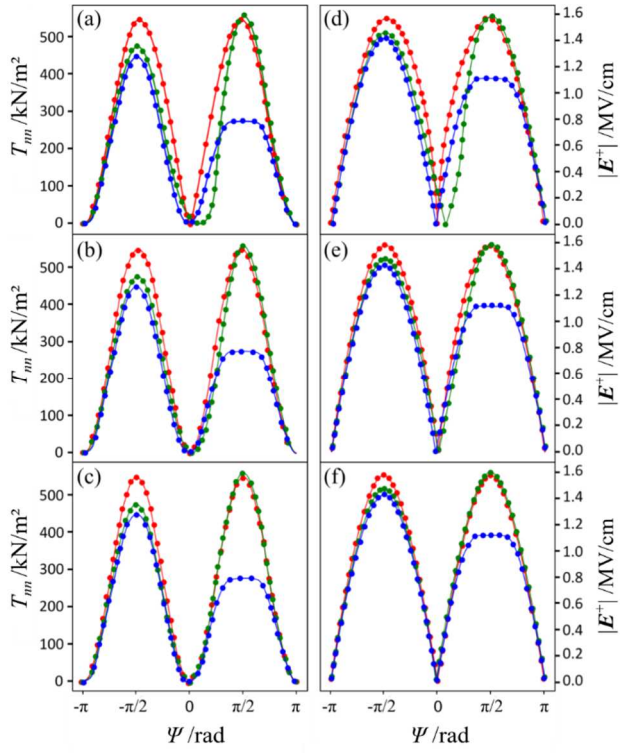

Fig. 4: (a)-(c) Comparison between $T_{nn}^{\pm}$ obtained using FM- (solid line) and TLA- (dots) based model, where (a), (b) and (c) respectively correspond to values of φ={0, π/4, π/2} for a 2-cell configuration (with reference to Fig. A2 of appendix A). Green, red and blue curves respectively correspond to θ={0, π/4, π/2}, and r/R=0.2. (d)-(f) The same as in (a)-(c) for the $|\boldsymbol{E}^{\pm}|$.

In the additional Figs. A4 and A5 of appendix A, we present further calculations of the T_{nn} component of the MST and electric field imbalance for the 2-cell configuration and several choices of θ and φ, while all other initial conditions remain unchanged. It is interesting to note that the disparity in nominal value (shaded regions) of these quantities is much larger in FM-based calculations than in TLA-based analysis, which is consistent with the resolution limitations of the simulations using a FM-based approach for modeling 3D geometries. The T_{nn} component of the MST and electric field imbalances can then be strongly disturbed, and the net effect is that these quantities are changed very rapidly at $\psi=\pm\pi/2$. In contrast, the angular variation of these quantities are much precise within the TLA approach.

This observation immediately suggests that cells in close proximity change the local electric field distribution and create local non-uniformity in the electric field which eventually becomes more complex with an increase in the number of interacting cells [10]. All these "complications" could provide a gold mine of information about the formation of a stable biological tissue in space and time if an intuitive exploration of the realm of possibility for cell assemblies whose properties mimic those of real tissues is found. However, this observation having been made, no thorough investigation of the collective effects of neighboring cells on the details of the TMP and MST has been given. Since the physical aspects of the cellular environment that are sensed by cells are force and geometry at the nano-to micrometer level, these TLA-based simulations should allow us resolve some of the recent issues in understanding electromechanical couplings which triggers pore opening [11-14]. It is of interest that such extension of the single cell model can potentially lead to interesting coupling hierarchies of cells, which could also have important applications from the perspective of tissue ED modelling [34]. We leave this an open question.

To complete this analysis, we next turn to examine the impact of the electromechanical coupling (with reference to Fig. 2) characterizing the ED force during the deformed state of the cell, for which the prolate spheroidal shape of the cell has for effect to increase the membrane polarization, and consequently the local value of V_m. Here, we want to outline that the simple elasticity based analysis can be exploited to construct a complete picture of the local stress state surrounding the membrane. We show in Fig. 5 a comparison between selected deformed states of an initially (undeformed) spherically-shaped cell at three different times. In Figs. 5(a) and 5(b), V_m and the MST are calculated within a non-deforming mesh (no electromechanical coupling), while Fig. 5(c) is obtained with the TLA model by taking into account electromechanical coupling, i.e., the mesh deformation impacts the time dependent V_m and, in turn, the MST.

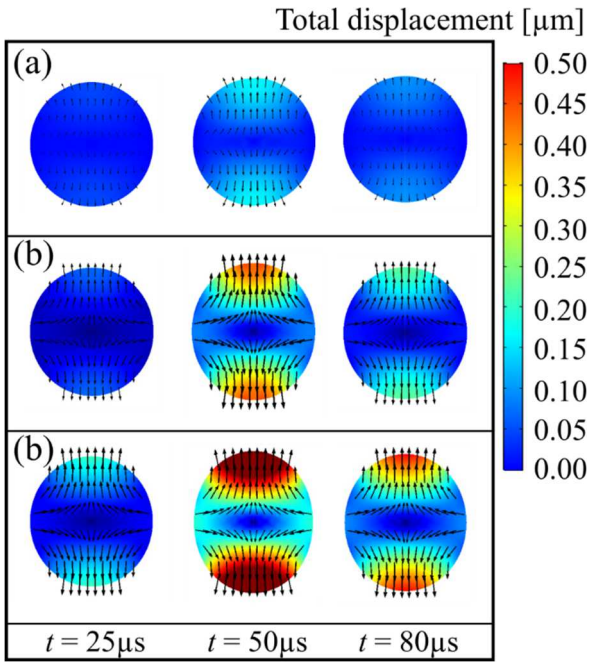

Fig. 5: Total cell displacement at three different times. The applied pulse is shown in Fig. A1 of Appendix A with intensity set to 1k V/cm: (a) FM results with no electromechanical coupling, (b) TLA results with no electromechanical coupling, and (c) TLA results with electromechanical coupling. The color bar shows the total displacement and the black arrows represent the direction of the displacement.

In addition to the challenge of consistently generating low computational time simulations, another well-documented test problem in the literature [8,14] can be used for the validation of the method outlined above. Besides determining the dependence of the local electric field and MST of the deformed cell, current strategies for analyzing ED focus on measuring the morphology change which is a generic feature of cell deformation. To confirm our approximate results, we show an example of such comparison in the top panel of Fig. 6 where we display the aspect ratio (defined as the ratio of semi-major axis b to semi-minor-axis a of the ellipsoid) of the ellipsoidal deformation for a single (initially spherical) reference cell configuration as a function of time.

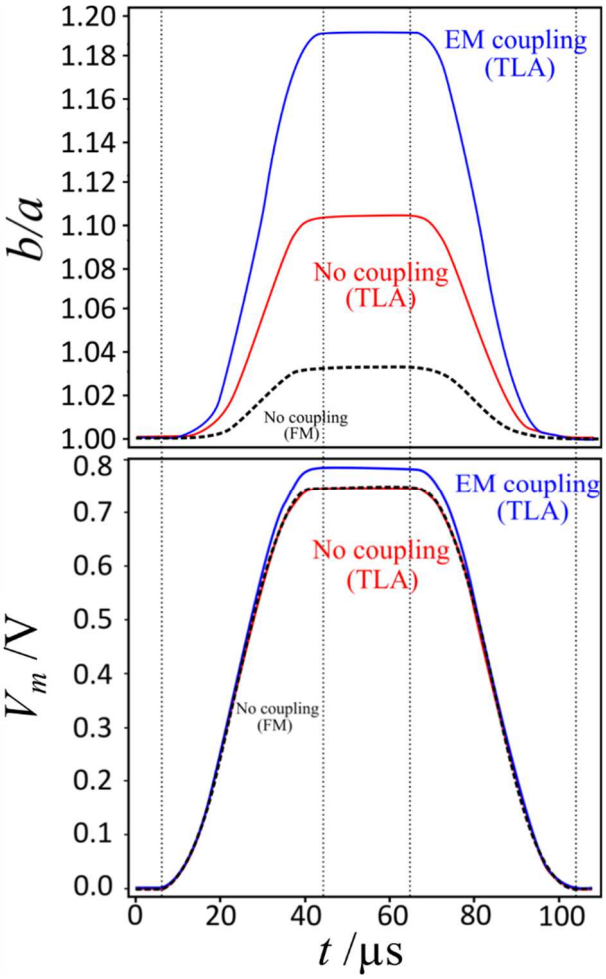

Fig. 6: (top panel) Evolution of the aspect ratio related to the ellipsoidal deformation of the initially spherical cell (Fig. 1) as a function of time. (bottom panel) The same as in the top panel for the transmembrane potential. Solid lines correspond to the TLA model. The blue (resp. red) color corresponds to the case when electromechanical coupling is (resp. is not) taken into account. The black dotted line corresponds to the FM model.

Figure 6 reinforces the strong correlation between deformation and the strain dependent evolution of V_m as a function of time. One can note that the steady state value of maximal deformation is reached in both cases closely after the end of the rise of the electric pulse. Moreover, in the coupled case, the steady state value of V_m depends on the on the mechanical properties of the cell. The important point is that as long as the inequality $V_m<1$ is satisfied, the TLA-based analysis implicitly takes into account the global symmetry breaking by cell

ED which is under perturbative control. Now comparing the FM and TLA methods when electromechanical coupling is not taken into account, one can also notice that the two models predict significant differences. These difference range from 7 % when one considers the aspect ratio (Fig. 6) to 200% when the time-dependent total cell displacement (Fig. 5) is analyzed. One can rationalize this point as due to the normal strains in the FM model and the large elastic modulus ratio between the cytoplasm and the membrane. In the FM model, electrostriction effects are found to induce a membrane shrinking up to 5% of its initial thickness [26]. Therefore, neglecting electrostriction in the TLA formulation of Eqs.(20)-(24), while imposing similar electromechanical constraints as in the FM model, should result in an excess mechanical energy (mainly stored in the membrane) leading to a larger total strain in the TLA method.

We find another interesting application of TLA. The ED theory predicts the degree of deformation *b/a* induced on the reference cell when applying the trapezoidal electric pulse (Fig. A1) and electrical conductivity ratio Λ of the cytoplasm to the extracellular medium (ECM). Refs. [8,14] worked out the implication of the more or less conductive ECM constraint for the aspect ratio. Their result is that the cell evidences an oblate deformation when $\Lambda<1$ and prolate when is oblate when $\Lambda>1$. This is clearly consistent with the results displayed in Fig. 7.

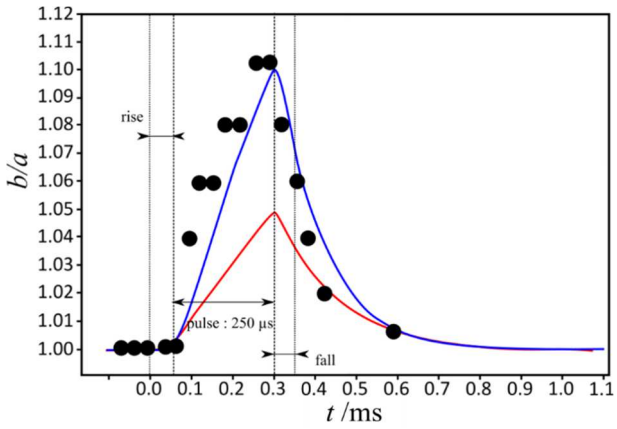

Fig. 7: Evolution of the aspect ratio characterizing the ellipsoidal deformation of an initially spherical vesicle as a function of time. We present our results in terms of benchmark points for vesicle deformation since we compare experimental results (black dots) [14] and numerical results (blue solid line) based on the TLA approach or the FM model (red solid line). In [14], a non electroporated vesicle in low conducting aqueous environment is subjected to an electric pulse of duration 250 μs and intensity 1 kV/cm [14]. The parameters used in the TLA model for producing this figure are summarized in Table I of appendix A.

As can be seen in the TLA-based calculations shown in Fig. 7 are in good agreement with the experimental data on giant unilamellar vesicules [8,14], which are representative models of cells since they have similar dimension and can be individually observed and followed with video microscopy. It should be remarked that for this benchmark model, the experimental parameters used in the TLA model for producing this figure are summarized in Table I. Thus remarkably, we confirm our approximate results are relevant to describe the large cell deformations under electromechanical excitation. In fact, our TLA procedure by integrating ED in the analysis gives us a large flexibility since the physical parameters in the model we present are linked to scales we know should be associated with deformation, bending rigidity,

and elastic stretching mechanisms. The details of this process are currently under investigation.

IV. CONCLUSIONS

One of the key features of this approach is it allows for addressing the electromechanical coupling that can give rise to visible signatures arising from two cells in close proximity, with the specific signal depending on the particular nature of this coupling. Since a wild range of possible experiments can be proposed, it is very important to ascertain exactly what signals may be expected as a function of electric field excitation and ECM characteristics. For all test cases, our arguments suggest that the use of TLA offers significant computational advantage over solving the FM description of the cell membrane. This claim is substantiated by means of several examples showing how this method can be exploited in multiscale simulations of biological tissue on cellular and subcellular scale. Furthermore, some well-known benchmark tests have been performed to validate the accuracy, efficiency, and computational time of the proposed method. It certainly appears that while there are quantitative differences between the TLA-based approach and FM, the former simulates the essential trends of realistic or observed ED behavior under direct current electric field. The electromechanical strategy was demonstrated to be accurate with only moderate computational expense, and it should perhaps be emphasized once again that our method showed good agreement with available experimental and numerical results in the literature.

Given this discussion, it is useful to keep in mind several specific challenges that we should unravel in the foreseeable future. One of the greatest impacts of continuum simulations is that they offer an intuitively simple, yet physically complete model of biological cells. As an alternative to finite element simulations the boundary integral equation method offers important advantages to solve linear field problems since a surface description of the modeled object is sufficient. To solve for the potential, this method has computation cost. However, adaptive meshing covering the region of interest combined to the boundary integral method makes the method fast as well as accurate [38]. We leave this an open question. Furthermore, numerous features such as inhomogeneous thin-layer (membrane) and generalization to either high-frequency time harmonic or transient electric field excitations have so far received very little attention. The former issue requires combining the actual TLA with homogenization problems. The latter issue turns out to be technically more difficult, in particular regarding the stability in time. We wish also to notice that a priori, this new strategy can be transferred in a straightforward manner to viscoelastic or hyperelastic membrane if the corresponding material properties are known [29,31]. It then makes sense to ask if and how the TLA is an appropriate approach for all types of eukaryotic cells. Another major milestone for this research would be to use this computational method to deal with EP of cell membrane in order to extract specific metrics such as pore density and elastic strain energy [12-13,17,35-37,39]. We leave these questions for future studies.

Data availability

The data that support the findings of this study are available from the corresponding author upon reasonable request.

Acknowledgment

E. S. would like to thank Université de Brest for supporting this research through its PhD program. This work was performed under the auspices of the Lab-STICC which is the Unité Mixte de Recherche CNRS 6285.

Appendix A: Technical details

The purpose of this appendix is to present the type of electric pulse excitation, the geometry of each model for the TLA-based approach and FM analysis, the electric pulse characteristics, and additional results.

Electric field excitation is provided by a unipolar trapezoidal pulse having amplitude of 1 kV/cm with rise-and fall-times set to 1.25 μs as shown in Fig. A1.

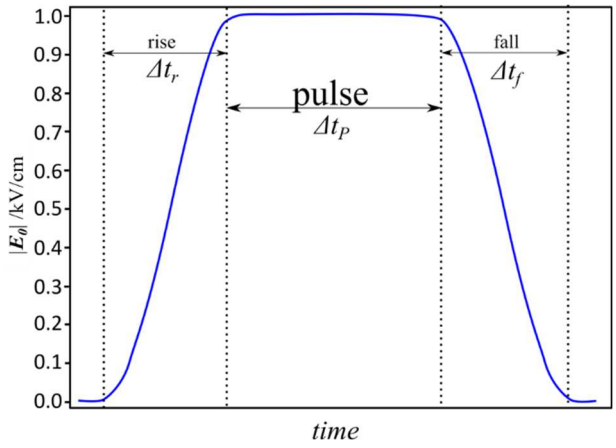

Fig. A1: The electric pulse excitation applied in this study. The pulse intensity is set to 1kV/cm. The values of the rise, pulse, and fall times are listed in Table AI.

We show in Fig. A2 the geometry of the 1-cell and 2-cell configurations considered in this analysis.

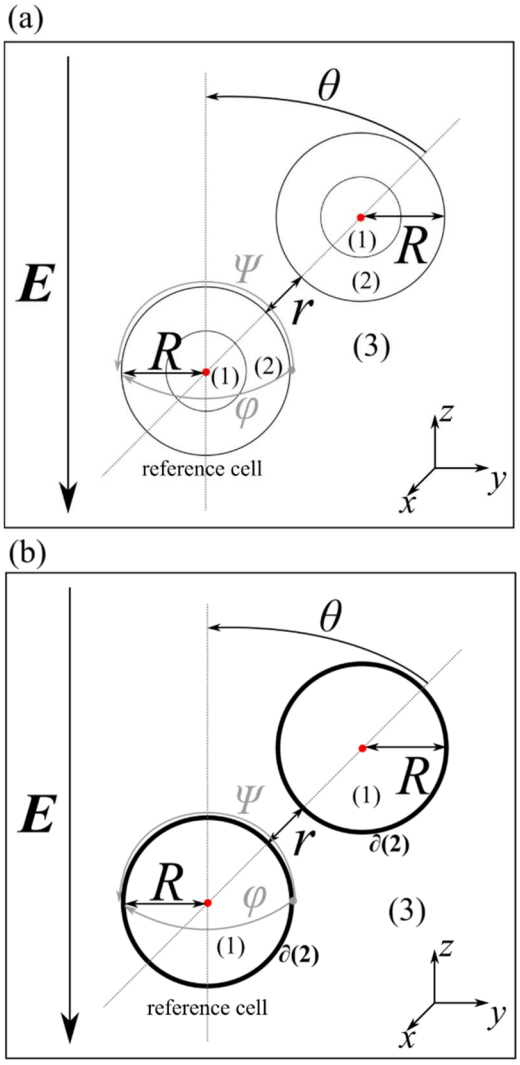

Fig. A2: (a) A schematic diagram illustrating the geometry of the problem (not to scale) for the TLA and FM of the reference cell for the 2-cell configuration (3D geometry). For the latter, the two cells are separated by a distance r. The orientation angle θ refers to the angle of the line joining the cell centers of mass relative to the electric field direction. Red dots represent the centers of mass of the cells, and regions (1), (2) or $\partial(2)$ and (3) respectively correspond to cytoplasm, membrane and external medium. As shown in this figure, by considering different values of r and θ we can assign arbitrary electromechanical coupling and anisotropies to the pair of cells configuration. We have also defined ψ and φ as the angles starting from point $(x_0; y_0 + R; z_0)$ and contained in the zOy plane and xOy plane, respectively, where $(x_0; y_0; z_0)$ are the coordinates of the center of mass of the reference cell; (b) The same as in (a) for the TLA-based approach.

Table II summarizes the parameters used in the FE analysis of biological cells exposed to electric fields. It also includes the electric pulse (Fig. A1) characteristic times.

Table II: A summary of the parameters used in the TLA and FM models for producing the specified figures.

Parameters	Notation	Fig. 3	Fig. 4	Figs. 5 and 6	Fig. 7
Cell (vesicle) radius (in the undeformed state)	R (μm)	5	5	5	15
Membrane thickness of the undeformed cell (vesicle)	d_{m0} (nm)	5	5	5	5
Cytoplasm permittivity	$\varepsilon_0\varepsilon_c$ (Fm^{-1})	6.9×10^{-10}	6.9×10^{-10}	6.9×10^{-10}	5.6×10^{-10}
Cytoplasm conductivity	σ_c (Sm^{-1})	0.2	0.2	0.2	6×10^{-4}
Membrane permittivity	$\varepsilon_0\varepsilon_m$ (Fm^{-1})	4.4×10^{-11}	4.4×10^{-11}	4.4×10^{-11}	4.4×10^{-11}
Membrane conductivity	σ_m (Sm^{-1})	10^{-7}	10^{-7}	10^{-7}	10^{-7}
External medium permittivity	$\varepsilon_0\varepsilon_e$ (Fm^{-1})	6.9×10^{-10}	6.9×10^{-10}	6.9×10^{-10}	5.6×10^{-10}
External medium conductivity	σ_e (Sm^{-1})	0.2	0.2	0.2	4.5×10^{-4}
Membrane Young modulus	Y_m (Pa)	1.9×10^{7}	1.9×10^{7}	1.5×10^{7}	1.5×10^{7}
Cytoplasm Young modulus	Y_c (Pa)	10^{3}	10^{3}	10^{2}	10^{2}
Rise time	Δt_r (s)	1.25×10^{-6}	-	4×10^{-5}	2.5×10^{-5}
Pulse time	Δt_P (s)	2.5×10^{-5}	-	2×10^{-5}	2.5×10^{-4}
Fall time	Δt_f (s)	1.25×10^{-6}	-	4×10^{-5}	2.5×10^{-5}

To compare the outputs of the FM and TLA models for 2D and 3D configurations, the convergence study is based on the analysis of the number of edge elements N_m on each membrane interface. The minimum and maximum element size parameters are the only required inputs parameters in order to build the mesh from the built-in discretization algorithm they were respectively set to R/N_m and $100R/N_m$ for the 2D geometries and to R/N_m and $1000R/N_m$ for the 3D geometries. The total relative error reads

$$\frac{\int_{C_{ref.cell}} T_{nn}(N_m) - T_{nn}(N_m = N_{m_{max}})\, dl}{\int_{C_{ref.cell}} T_{nn}(N_m = N_{m_{max}})\, dl} = \xi. \qquad \text{(A1)}$$

Here, $\int_{C_{ref.cell}} dl$ represents the integral over the cell contour in a 2D geometry or over the reference cell contour taken at $\varphi = 0$ in a 3D geometry. The threshold value of the total relative error is fixed to 0.5% and Fig. A3 shows the mesh values at which this criterion is reached, where $N_{m_{max}}$ is chosen to have a sufficient high value so that the mesh quality would a priori satisfy the required stability conditions for computing an accurate approximated

solution. Here, the results of the FM model for a 3D geometry are not shown since the algorithm used to build the mesh cannot discretize the system in order it leads to the required level of accuracy in a reasonable amount of time. A value of $N_{m_{max}} = 50\ 000$ was chosen for this illustrative example.

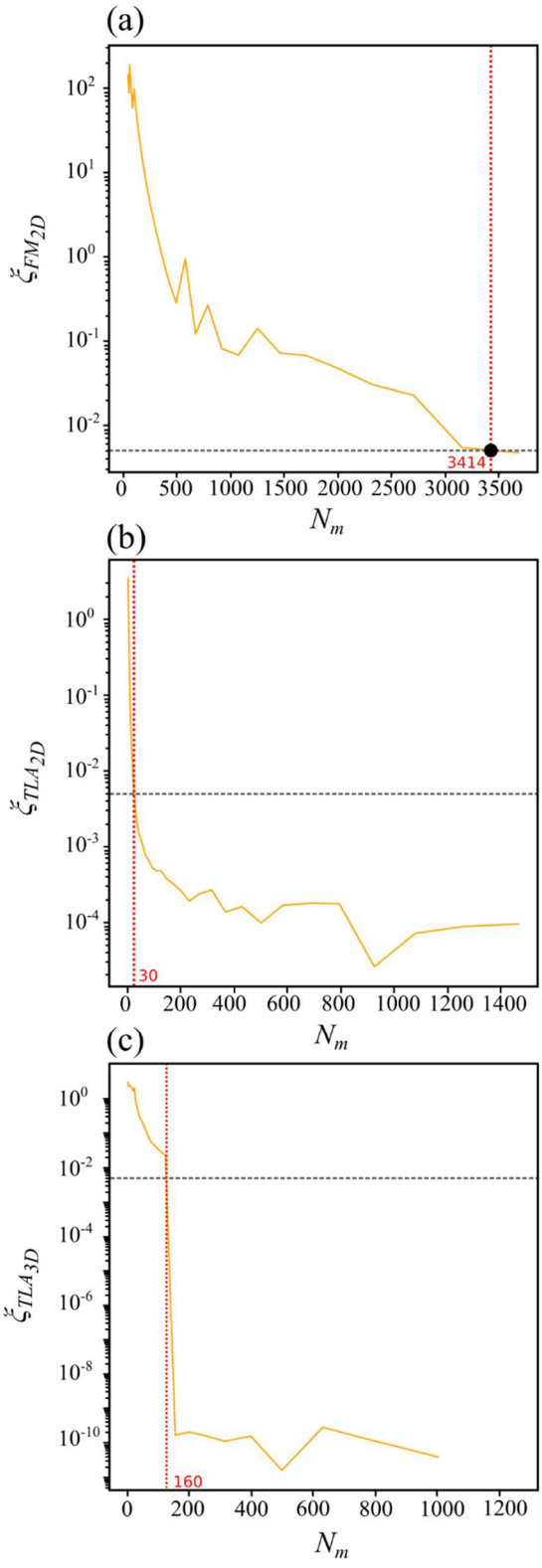

Fig. A3: Dependence of the relative error ξ as a function of the total number of mesh elements N_m used to discretize the system: (a) FM results in 2D with $N_{m_{max}} = 4640$, (b) TLA results in 2D with $N_{m_{max}} = 1232$, (c) TLA results in 3D with $N_{m_{max}} = 1232$. The grey dotted line represents the case ξ = 0.5 %. The red dotted vertical line represents the critical value of N_m beyond which the approximated solution can be considered as mesh-independent.

In Figs. A4 and A5, we show additional results which are discussed in the main text. It is worth observing the instability of the FM results shown in Figs. A4 and A5.

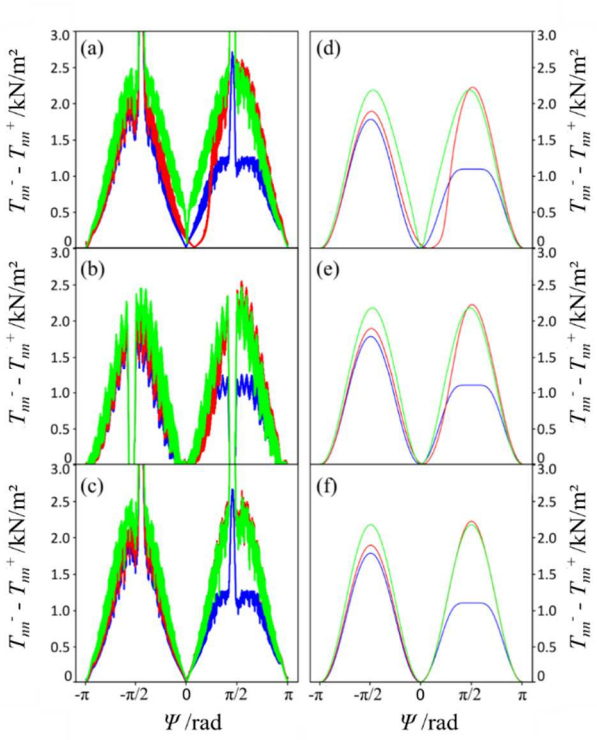

Fig. A4: (a)-(c) Angular variation of the transmembrane imbalance of the MST for the 2-cell configuration within the FM model: (a), (b) and (c) respectively correspond to values of φ={0, π/4, π/2}. Green, red and blue curves respectively correspond to θ={0, π/4, π/2}, r/R=0.2; (d)-(f) The same as in (a)-(c) for the TLA model.

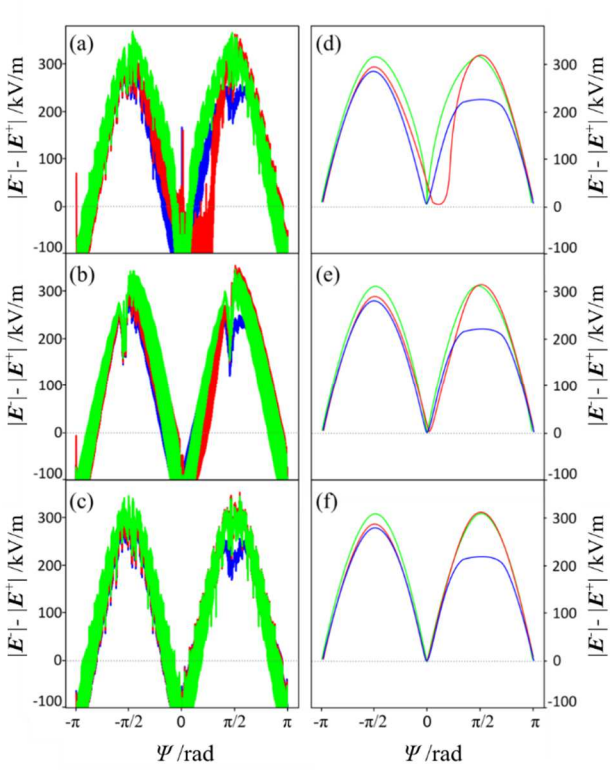

Fig. A5: The same as in Fig. A4 for the transmembrane imbalance of the norm of the electric field.

REFERENCES

[1] P. M. A. Sloot and A. G. Hoekstra, "Multi-scale modelling in computational biomedicine", Briefings in Bioinformatics **11**, 142–152 (2010).
[2] S. Schnell, R. Grima, and P.K. Maini, "Multiscale modeling in biology", American Scientist **95**, 134-142 (2007).
[3] C. Brosseau and E. Sabri, "Resistor-capacitor modelling of the cell membrane: a multiphysics analysis", J. Appl. Phys. **129**, 011101 (2021).
[4] J. O. Dada and P. Mendes, "Multi-scale modelling and simulation in systems biology", Integr. Biol **3**, 86-9 (2011).
[5] M. Meier-Schellersheim, I. D. C. Fraser, and F. Klauschen, "Multi-scale modeling in cell biology", Wiley Interdiscip. Rev. Syst. Biol. Med. **1**, 4–14 (2009).
[6] D. Shamoon, S. Lasquellec, and C. Brosseau, "Perspective: Towards understanding the multiscale description of cells and tissue by electromechanobiology", J. Appl. Phys. **123**, 2018, 240902(1)-240902(18).
[7] N. A. Nodargi, P. Bisegna, and F. Casellin, "Effective computational modeling of erythrocyte electro-deformation", Meccanica **52**, 613-631 (2017).
[8] J. Chen, M. Abdelgawad, L. Yu, N. Shakiba, W.- Y. Chien, Z. Lu, W. R. Geddie, M. A. S. Jewett, and Y. Sun, "Electrodeformation for single cell mechanical deformation", J. Micromech. Microeng. **20**, 065007 (2010).
[9] F. Guo, K. Qian, H. Deng, and X. Li, "Multiphysics analysis of nsPEF induced electrodeformation in a dispersive cell model", Appl. Phys. Lett. **118**, 083701 (2021).
[10] D. Shamoon, J. Dermol-Cerne, L. Rems, M. Rebersek, T. Kotnik, S. Lasquellec, C. Brosseau, and D. Miklavčič, "Assessing the electro-deformation and electro-permeabilization of biological cells using a three dimensional finite element model", Appl. Phys. Lett. **114**, 2019, 063701(1)-063701(5); D. Shamoon, S. Lasquellec, and C. Brosseau, "A muliphysics analysis of the strain energy in multicellular environments", Appl. Phys. Lett. **115**, 043701 (2019).
[11] A. Barnett and J. C. Weaver, "Electroporation: a unified quantitative theory of reversible electrical breakdown and mechanical rupture in artificial planar bilayer membranes", Bioelectrochem. Bioenerg. **25**, 163-182 (1991); J. C. Weaver and Y. Chimazdzhev, "Theory of electroporation: a review", Bioelectrochem. Bioenerg. **41**, 135-160 (1996).
[12] L. Rems and D. Miklavčič, "Tutorial: Electroporation of cells in complex materials and tissue", J. Appl. Phys. **119**, 201101 (2016).
[13] J. C. Weaver and Y. A. Chizmadzhev, "Theory of electroporation: A review", Bioelectrochemistry and Bioenergetics **41**, 135-160 (1996).
[14] K. A. Riske and R. Dimova, "Electro-deformation and poration of giant vesicles viewed with high temporal resolution," Biophys. J. **88**, 1143–1155 (2005).
[15] U. Pliquett, R. P. Joshi, V. Sridhara, and K. H. Schoenbach, "High electrical field effects on cell membranes," Bioelectrochemistry **70**, 275–282 (2007).
[16] M. M. Sadik, J. Li, J. W. Shan, D. I. Shreiber, and H. Lin, "Vesicle deformation and poration under strong dc electric fields," Phys. Rev. E **83**, 066316 (2011).
[17] E. Goldberg, C. Suarez, M. Alfonso, J. Marchese, A. Soba, and G. Marshall, "Cell membrane electroporation modeling: A multiphysics approach", Biolectrochemistry **124**, 28-39 (2018).
[18] E. Fear and M. Stuchly, "Modeling assemblies of biological cells exposed to electric fields", IEEE Trans. Biomed. Eng. **45**, 1259–1271 (1998).
[19] G. Pucihar, T. Kotnik, B. Valic, and D. Miklavcic, "Numerical determination of transmembrane voltage induced on irregularly shaped cells", Ann. Biomed. Eng. **34**, 642–652 (2006).

[20] C. Poignard, P. Dular, R. Perrussel, L. Krähenbühl, L. Nicolas, and M. Schatzman, "Approximate conditions replacing thin layers", IEEE Trans Magn. **44**, 1154-1157 (2008).
[21] A. Morshed, P. Dutta, M. R. Hossan, and R. Dillon, "Electrodeformation of vesicles suspended in a liquid medium", Phys. Rev. Fluids **3**, 103702 (2018)
[22] W. F. Hu, M. C. Lai MC, Y. Seol, and Y. N. Young, "Vesicle electrohydrodynamic simulations by coupling immersed boundary and immersed interface method", J. Comput. Phys. **317**, 66 (2016).
[23] J. Chen, M. Abdelgawad, L. Yu, N. Shakiba, W.-Y. Chien, Z. Lu, W. R Geddie, M. A. S. Jewett, and Y. Sun, "Electrodeformation for single cell mechanical characterizations", J. Micromech. Microeng. **21**, 054012 (2011).
[24] H. Nganguia and Y.-N. Young, "Equilibrium electrodeformation of a spheroidal vesicle in an AC electric field", Phys. Rev. E **88**, 052718 (2013).
[25] K. Asami, "Effectiveness of thin-layer and effective medium approximations in numerical simulation of dielectric spectra of biological cell suspensions", Jpn. J. Appl. Phys. **49**, 127001 (2010).
[26] E. Sabri, S. Lasquellec, and C. Brosseau, "Electromechanical modeling of the transmembrane potential-dependent cell membrane capacitance", Appl. Phys. Lett. **117**, 043701 (2020).
[27] E. Sabri and C. Brosseau, "Proximity-induced electrodeformation and membrane capacitance coupling between cells", Eur. Biophys. J. **50**, 713-720 (2021).
[28] E. Sabri and C. Brosseau, "Modelling cell membrane electrodeformation by alternating electric fields", Phys. Rev. E (2021).
[29] P.- Y. Chen, A. Lin, and Y. Seki, "Biological materials: Structure and mechanical properties", Prog. Mater. Sci. **53**, 1-206 (2008).
[30] I. G. Abidor, V. B. Arakelyan, L.V. Chernomordik, Y. A. Chizmadzhev, V. F. Pastushenko, and M. R. Tarasevich, "Electric breakdown of bilayer lipid membranes. I. The main experimental facts and their qualitative discussion", Bioelectrochem. Bioenerg. **6**, 37-52 (1979); M. Tarek, "Membrane electroporation: a molecular dynamics simulation", Biophys. J. **88**, 4045-4053 (2005); Z. Q. Levine and P. T. Vernier, "Life cycle of an electropore: Field-dependent and field-independent steps in pore creation and annihilation", J. Memb. Biol. **226**, 27-36 (2010); E. Gongadze, A. Velikonja, S. Perutkova, P. Kramar, A. Maček-Lebar, V. Krajl-Iglič, and A. Iglič, "Ions and water molecules in an electrolyte solution in contact with charged and dipolar surfaces", Electrochimica Acta **126**, 42-60 (2014).
[31] C. J. Cyron, K. W. Müller, A. R. Bausch, and W. A. Wall, "Micromechanical simulations of biopolymer networks with finite elements", J. Comput. Phys. **244**, 236-251 (2013) ; D. Barthès-Biesel, A. Diaz, and E. Dhenin, "Effect of constitutive laws for two-dimensional membranes on flow-induced capsule deformation", J. Fluid Mech. **460**, 211-222 (2002).
[32] J. Vodman, "Electric forces for microscale cell manipulation", Annu. Rev. Biomed. Eng. 8, 425-454 (2006).
[33] V. Sukhorukov, H. Mussauer, and U. Zimmermann, "The effect of electrical deformation forces on the electropermeabilization of erythrocyte membranes in low- and high-conductivity media", J. Membr. Biol. **163**, 235-245 (1998).
[34] T. Murovec, D. C. Sweeney, E. Latouche, R. V. Davalos, and C. Brosseau, "Modeling of transmembrane potential in realistic multicellular structures before electroporation", Biophys. J. **111**, 2286-2295 (2016); T. Murovec and C. Brosseau, "Spectral fingerprint of electrostatic forces between biological cells", Phys. Rev. E, **92**, 2015, 042717.
[35] K. Ravikumar, V. Kumaran, and B. Basu, "Biophysical implications of Maxwell stress in electric field stimulated cellular microenvironment on biomaterial substrates", Biomaterials **209**, 54-66 (2019).

[36] J. Gimsa, "A comprehensive approach to electro-orientation, electrodeformation, dielectrophoresis, and electrorotation of ellipsoidal particles and biological cells", Bioelectrochemistry **54**, 23–31 (2001).
[37] COMSOL Multiphysics version 5.5.
[38] W. Ying and J. T. Beale, "A fast accurate boundary integral method for potentials on closely packed cells", Commun. Comput. Phys. **14**, 1073-1093 (2013); L. C. McConnell, M. J. Miksis, and P. M. Vlahovska, "Continuum modeling of the electric-field-induced tension in deforming lipid vesicles", J. Chem. Phys. **143**, 243132 (2015); C. Sorgentone, A.-K. Tornberg, and P. M. Vlahovska, "A 3D boundary integral method for the electrohydrodynamics of surfactant-covered drops", J. Comp. Physics, **389**, 111-127 (2019) ; S. A. Sauter, C. Schwab, *Boundary Element Methods* (Springer, 2011) ; C. Pozrikidis, *Boundary Integral and Singularity Methods for Linearized Viscous Flow* (Cambridge University Press, 1992).
[39] A. G. Pakhomov, J. F. Kolb, J. A. White, R. P. Joshi, S. Ziao, and K. H. Schoenbach, "Long-lasting membrane permeabilization in mammalian cells by nanosecond pulsed electric field (nsPEF)", Bioelectromagnetics **28**, 655-663 (2007); A. G. Pakomov, E. Gianulis, P. T. Vernier, I. Semenov, S. Xiao, and O. Pakhomova, "Multiple nanosecond electric pulses increase the number but not the size of long-lived nanopores in the cell membrane", Biochim. Biophys. Acta **1848**, 958-966 (2015).